Cancer Research

Snail1-Expressing Fibroblasts in the Tumor Microenvironment Display Mechanical Properties That Support Metastasis

Jelena Stanisavljevic[1], Jordina Loubat-Casanovas[1], Mercedes Herrera[2], Tomás Luque[3,4], Raúl Peña[1], Ana Lluch[5,6], Joan Albanell[7,8,9], Félix Bonilla[2], Ana Rovira[7,8], Cristina Peña[2], Daniel Navajas[3,4,12], Federico Rojo[7,10,11], Antonio García de Herreros[1,9], and Josep Baulida[1]

Abstract

Crosstalk between tumor and stromal cells in the tumor microenvironment alter its properties in ways that facilitate the invasive behavior of tumor cells. Here, we demonstrate that cancer-associated fibroblasts (CAF) increase the stiffness of the extracellular matrix (ECM) and promote anisotropic fiber orientation, two mechanical signals generated through a Snail1/RhoA/αSMA–dependent mechanism that sustains oriented tumor cell migration and invasiveness. Snail1-depleted CAF failed to acquire myofibroblastic traits in response to TGFβ, including RhoA activation, αSMA-positive stress fibers, increased fibronectin fibrillogenesis, and production of a stiff ECM with oriented fibers. Snail1 expression in human tumor–derived CAF was associated with an ability to organize the ECM. In coculture, a relatively smaller number of Snail1-expressing CAF were capable of imposing an anisotropic ECM architecture, compared with nonactivated fibroblasts. Pathologically, human breast cancers with Snail1^{+} CAF tended to exhibit desmoplastic areas with anisotropic fibers, lymph node involvement, and poorer outcomes. Snail1 involvement in driving an ordered ECM was further confirmed in wound-healing experiments in mice, with Snail1 depletion preventing the anisotropic organization of granulation tissue and delaying wound healing. Overall, our results showed that inhibiting Snail1 function in CAF could prevent tumor-driven ECM reorganization and cancer invasion. *Cancer Res; 75(2); 284–95. ©2014 AACR.*

Introduction

Myofibroblasts are activated fibroblasts that remodel connective tissues in processes, such as development and wound healing (1, 2). They typically contain contractile αSMA (smooth muscle alpha actin)-positive stress fibers linked to and required for the formation of supermature integrin focal contacts, named fibronexus. Fibronexus transmits intracellular tensional forces to extracellular fibronectin molecules, allowing their assemblage into fibers (3). Extracellular fibronectin fibers facilitate and guide the polymerization of other molecules, such as thrombospondin-1, perostin, tenascin C (4), fibrillin, and collagen (5), into the extracellular matrix (ECM).

αSMA-positive stress fibers also connect intercellular cadherin junctions that permit them to withstand mechanical stress between neighbor cells; indeed, adherens junctions of cultured myofibroblasts are significantly larger than those of αSMA-negative fibroblasts (6). The ECM architecture of connective tissues and the myofibroblast phenotype, including nuclei (7) and cell shapes (3), ultimately depend on an intraextracellular tensional dialog mediated by these specialized cell–substrate and cell–cell structures.

Cancer-associated fibroblasts (CAF) are a heterogeneous population of activated fibroblasts whose activity in the stroma associates with tumor progression and malignancy. CAFs produce paracrine growth factors, proteolytic enzymes, and ECM components, and contribute to generate a desmoplastic response (fibrillar network deposition) around cancer cells (8) similar to that at the granulation tissue of wounds. Thus, CAF activity perturbs not only the biochemical but also the biomechanical homeostasis of the tumor microenvironment; these perturbances are sensed by tumor cells and ultimately affect their behavior (9). In breast cancer, mechanical properties of the stroma, such as stiffness (10) and fiber alignment (11), force progression of the disease. In fact, the presence of dense and aligned collagen fibers around human breast carcinomas is a prognostic signature for poor survival (12, 13). CAFs are permanently activated by a TGFβ autocrine loop (14), and

[1]Programa de Recerca en Càncer, Institut Hospital del Mar d'Investigacions Mèdiques, Barcelona, Spain. [2]Department of Medical Oncology, Puerta de Hierro Majadahonda University Hospital, Majadahonda, Madrid, Spain. [3]Unitat de Biofísica i Bioenginyeria, Universitat de Barcelona, Barcelona, Spain. [4]Institute for Bioengineering of Catalonia, Barcelona, Spain. [5]Department of Oncology and Hematology, Hospital Clínico Universitario, Valencia, Spain. [6]Department of Medicine, Valencia Central University, Valencia, Spain. [7]Molecular Therapeutics and Biomarkers in Cancer Laboratory, Institut Hospital del Mar d'Investigacions Mèdiques, Hospital del Mar, Barcelona, Spain. [8]Medical Oncology Department, Hospital del Mar, Barcelona, Spain. [9]Departament de Ciències Experimentals i de la Salut, Universitat Pompeu Fabra, Barcelona, Spain. [10]Department of Pathology, IIS-Fundación Jiménez Díaz, Madrid, Spain. [11]Department of Pathology, Hospital del Mar, Barcelona, Spain. [12]Ciber Enfermedades Respiratorias (CIBERES), 07110-Bunyola, Spain.

Note: Supplementary data for this article are available at Cancer Research Online (http://cancerres.aacrjournals.org/).

Corresponding Author: Josep Baulida, IMIM, C/Dr. Aiguader, 88, 08003, Barcelona, Spain. Phone: 34-3-316-0436; Fax: 34-3-316-0410. E-mail: jbaulida@imim.es

doi: 10.1158/0008-5472.CAN-14-1903

metastasis initiation in colorectal cancer is dependent on a TGFβ-driven program in stromal cells (15). TGFβ treatment induces activation of RhoA, a GTPase that promotes stress fiber formation, as well as αSMA synthesis, the assembly of which into stress fibers is necessary for efficient ECM remodeling (16, 17). No pathway accounting for rapid RhoA activation by TGFβ has been clearly defined.

Snail1 was initially described as a TGFβ target that promotes the epithelial-to-mesenchymal transition (EMT) and, despite the lack of conclusive *in vivo* data, has been postulated to be a prognostic factor for this capacity (18). Though adult fibroblast normally do not express Snail (19), Snail1-positive fibroblast were described in wound healing and in the stroma of malignant colonic tumors (20). Cultured fibroblasts acquire three-dimensional (3D) invasion programs (21), and primary CAFs lines produce soluble biochemical signaling (22), in a Snail-dependent manner. However, molecular pathways modulated by Snail1 in fibroblasts are poorly defined, and no links between Snail1 activity and the generation of mechanical signals have been proposed. We have previously describe that a set of ECM genes can be transcriptionally upregulated by Snail1 (23) in cultured epithelial cells undergoing EMT and fibroblasts. Here, we demonstrate that expression of Snail1 in fibroblasts is required for the activation of RhoA and the acquisition of a myofibroblastic phenotype. As a consequence, scattered Snail1-expressing fibroblasts impose a mechanical microenvironment needed for wound repair and malignant cancer progression.

Materials and Methods

Reagents

Reagents were from SIGMA (ROCK1 inhibitor Y27632, Y-0503; DAPI, D-9542; tamoxifen, T5648-SG; 4-hydroxytamoxifen, H6278; Alcian blue, A5268; ascorbic acid, A-4403; Alizarin Red S, 122777), Cytoskeleton, Inc. (soluble fibronectin, FNR02-A), Life Technolologies [Alexa Fluor 488 phalloidin, A12379; CellTracker Green CMFDA (5-Chloromethylfluorescein Diacetate), C 2925]), ROCHE (Trichrome III Blue Staining, 5279364001), PREPROTECH (human TGFβ1, 100-21B), and BIONOVA (DAPI-fluoromount G, 0100-20).

Cell Culture

Cells were grown in DMEM (Invitrogen) supplemented with 4.5 g/L glucose (Life Technologies), 2 mmol/L glutamine, 56 IU/mL penicillin, 56 mg/L streptomycin, and 10% FBS (GIBCO) and maintained at 37°C in a humid atmosphere containing 5% CO_2. Where indicated, cells were treated with 5 ng/mL of TGFβ1 (Peprotech). MDA231MB, Ela-MYC, and 1BR3G-Snail1–HA (23) cells were acquired from the repository stock of our center. Mouse embryonic fibroblasts (MEF) were previously established in our laboratory from a conditional knockout (KO) mouse, *Snai1*$^{del/flox}$ mice (24), and were transfected with CRE or control vector to create the *Snai1* control and KO MEFs. For rescue experiments, KO MEFs were infected with retroviruses using indicated mSnail1–HA (cDNA) constructs described elsewhere (25) and cloned into a PBABE vector using the BamHI/SalI sites. Infected cells were selected with puromycin (2 μg/mL), and exogenous Snail1 expression was confirmed by Western blot analysis with an anti-HA antibody. Where indicated, the ROCK1 inhibitor was added to the medium to final concentration of 10 μmol/L 24 hours before the experiment. Mesenchymal stem cell (MSC) control and KO for *Snail1* were obtained from *Snai1*$^{flox/del}$ mice (24), in which wild-type *Snai1* expression was preserved or depleted by transduction of a control retrovirus or a CRE plasmid, respectively.

Cancer-associated fibroblast establishment and culture

Fresh colon tumor samples were obtained from the Puerta de Hierro University Hospital of Majadahonda, Madrid, Spain. Informed written consent was obtained from all participants after an explanation of the nature of the study, as approved by the Research Ethics Board of Puerta de Hierro Majadahonda University Hospital. Tissue samples were cut into small pieces of approximately 2 to 3 mm^3 in size and seeded in FCS medium with 200 U/mL penicillin, 200 μg/mL streptomycin, 100 μg/mL gentamicin, and 2.5 g/mL amphotericin B. When outgrowths of fibroblasts appeared, the culture medium was replaced by FMB (Lonza) supplemented with FGM-2 Bulletkit (Lonza) to facilitate fibroblast growth. The remnants of the tissue were carefully washed away, and CAFs were routinely maintained in FBM medium at 37°C in a humid atmosphere containing 5% CO_2. To evaluate the CAF enrichment of the culture, vimentin and pan cytokeratin were analyzed by immunofluorescence (26).

Standard protocols for immunofluorescence, immunohistochemistry, RhoA-GTP pull-down, generation of 3D extracellular matrices (3D-ECM), migration, invasion, *in vivo* wound healing, fibronectin fibrillogenesis, Young's modulus (E), and cell differentiation were used (for details, see Supplementary Data). Analyses of tumor samples were also described in Supplementary Data.

Results

Snail1 is required for TGFβ-induced ECM remodeling

To study a putative role of fibroblastic Snail on ECM mechanics, we generated *in vivo*–like 3D-ECMs using control or *Snai1*-KO MEFs grown in the presence or absence of TGFβ (Snail1 depletion is shown in Fig. 2B). Matrices generated by KO MEFs contained fewer fibronectin fibers than matrices generated by control ones (Fig. 1A). In control MEFs, TGFβ increased the thickness of the 3D-ECM, and 50% of fibronectin fibers, predominantly those in the matrix upper layers, oriented anisotropically (Fig. 1A and B). In contrast, cytokine treatment failed to reorganize the fibronectin fibers in 3D-ECMs from *Snai1*-depleted MEFs (Fig. 1A and B). Nuclei orientation angle histograms clearly showed that only control MEFs treated with TGFβ were anisotropically organized (Fig. 1C). The lower degree of organization observed in KO relative to control MEFs was not due to a slower growth rate, as the number of KO and control MEFs in the 3D-ECM were similar. Moreover, KO MEFs still produced a poor 3D-ECM with disorganized fibers, even when a 5-fold greater amount of cells was used to deposit the 3D-ECM.

The requirements for Snail1 were confirmed by reexpressing an inactive (proline 2 mutated to alanine) or active Snail1 protein in KO MEFs. Although proteins were expressed equivalently in the nucleus (Fig. 1D and Supplementary Fig. S4D), only the active form rescued the TGFβ-induced alignment of nuclei and fibronectin fibers (Fig. 1D). An identical TGFβ/Snail1–dependent pattern was obtained in other mesenchymal cells that express endogenous Snail1 levels, such as MSCs isolated from mouse bone marrow (Supplementary Fig. S1A). In contrast with 3D-ECM fiber organization, early TGFβ-induced events, like SMAD phosphorylation, were found to be equivalent in these cells (24),

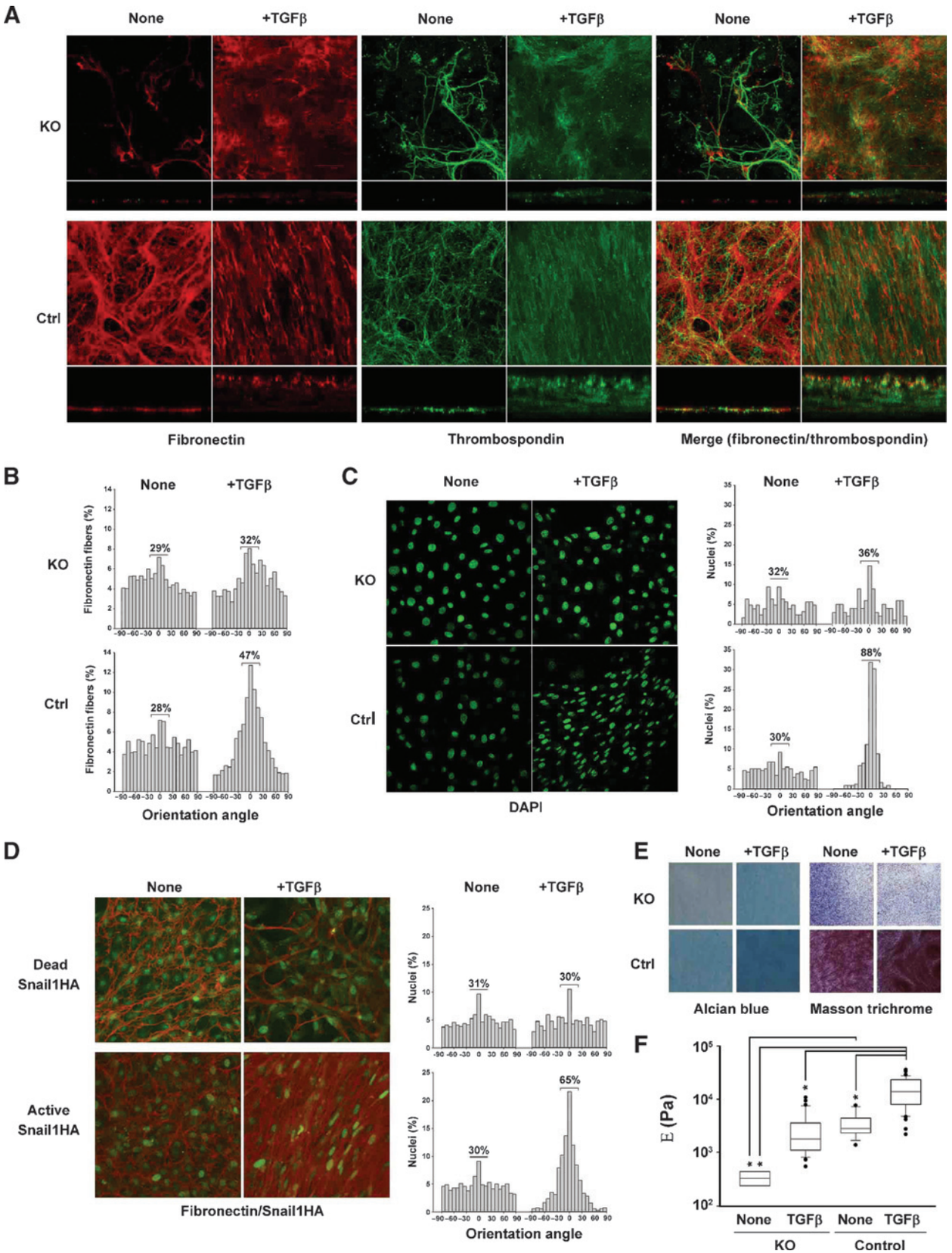

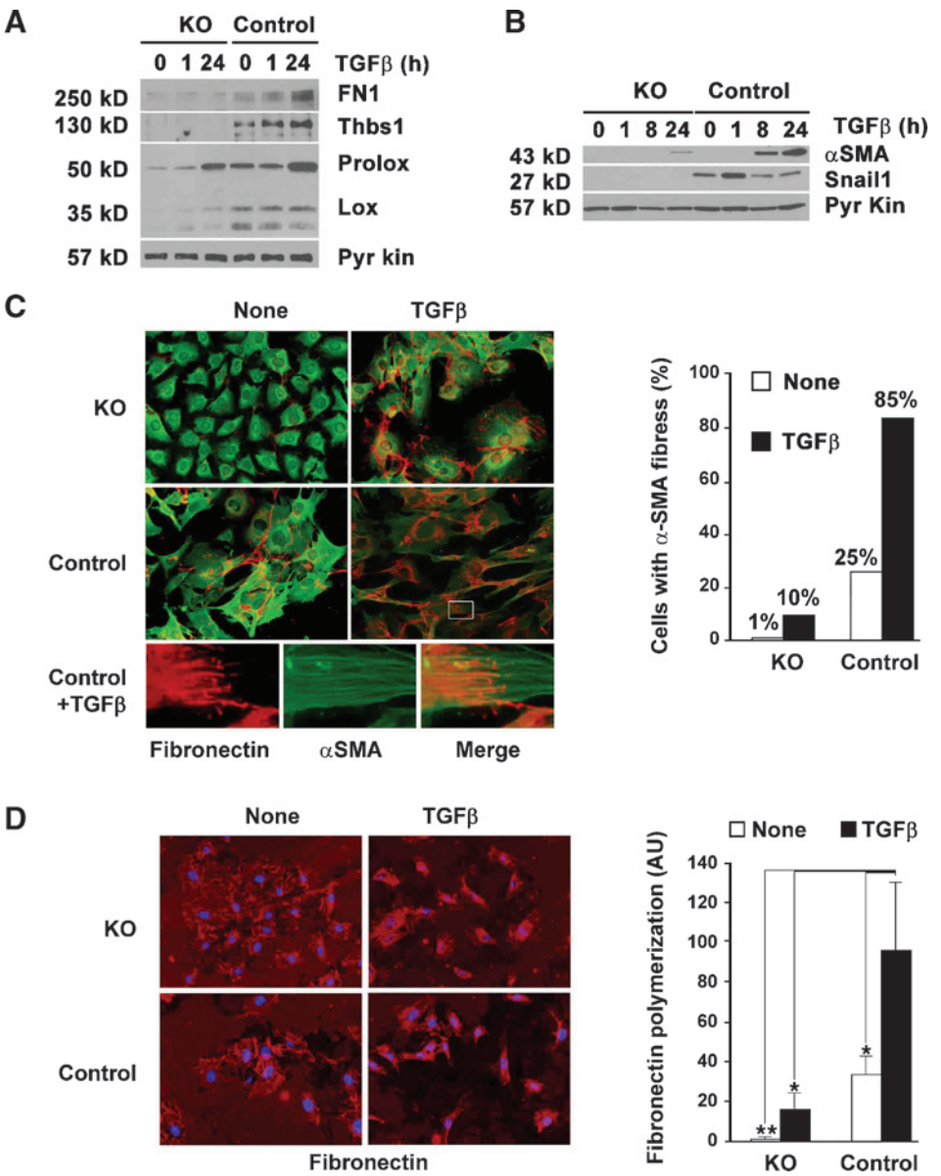

Figure 2.
Snail1 is required for TGFβ-induced αSMA expression and αSMA-dependent events. A, time course of thrombospondin, fibronectin, and LOX expression. Indicated protein levels were measured by Western blot analysis from total cell extracts of MEFs treated with TGFβ (5 ng/mL) at the indicated time points. Pyruvate kinase levels were measured as a loading control. B, time course of Snail1 and αSMA expression. The experiment was carried out and analyzed as in A. C, the percentage of MEFs with αSMA-positive fibers. αSMA fibers were visualized by immunofluorescence from MEFs grown in the presence or absence of 5 ng/mL of TGFβ1 for 60 hours (Supplementary Fig. S3A). Quantification of the percentage of MEFs with αSMA-positive fibers calculated from a minimum of 500 cells per condition. D, fibronectin fibrillogenesis by MEFs. Fibronectin was visualized by immunofluorescence after MEFs were cultured on fibronectin-coated cover slips for 16 hours (Supplementary Fig. S3D). The estimated fibrillogenesis in each condition is plotted. Bars, the mean ± SD from at least 10 different fields.

indicating that the deficient ECM organization in KO cells is not a consequence of a lower sensitivity to TGFβ. In addition, adult 1BR3G fibroblasts expressing ectopic Snail1 promoted a fiber alignment similar to that of activated MEFs (Supplementary Fig. S1B).

Congruent with the fact that fibronectin fibers prime the organization of other extracellular molecules, thrombospondin1 aligned parallel to fibronectin in the 3D-ECMs (Fig. 1A). Therefore, in addition to modulating the levels of ECM molecules, Snail1 is required to organize the extracellular fibrillar network. In

Figure 1.
TGFβ remodels the 3D-ECM generated by MEFs in a Snail1-dependent manner. A, fibronectin (green) and thrombospondin (red) fibers in 3D-ECMs. Fibers were visualized by immunofluorescence (at ×200) from the indicated MEFs treated or not with 5 ng/mL of TGFβ during 10 days of 3D-ECM deposition. A transversal 3D-ECM section is shown at the bottom. B, fibronectin fibers orientation in 3D-ECMs. Fibronectin fibers were visualized as in A and their orientation angles calculated (as indicated in Supplementary Methods using a described alogorith; ref. 43) and plotted as a frequency distribution. Percentages indicate oriented fibers accumulated in a range of ± 21° around the modal angle. C, nuclei orientation from control and *Snai1* KO MEFs. Nuclei were stained with DAPI in MEFs that had been treated as in A. The nuclei orientation angles were calculated (ImageJ) and frequency distribution plotted, as in B. D, ectopic Snail1 rescues the KO phenotype. Fibronectin (red) and Snail1 (green) were visualized from KO MEFs stability expressing a mouse Snail1-P2A (dead mutant) or Snail1-SA (active mutant) treated as in A. Nuclei were counterstained with DAPI and orientation angle frequencies plotted as in C. E, Alcian blue and Masson's trichrome staining. Images without magnification show representative regions of the indicated stained matrices. F, stiffness of extracellular matrices. Young's modulus. E, was estimated on decellularized matrices by atomic force microscopy and represented in a boxplot. Asterisks indicate a statistically significant difference as determined by ANOVA on ranks and Dunn method ($P < 0.001$).

fact, a major change of the 3D-ECM composition and rigidity is stimulated by TGFβ in a Snail1-dependent manner, as shown by staining of collagen- and acidic polysaccharide–containing molecules (Fig. 1E) and atomic force microscopy analysis (Fig. 1F). These changes in 3D-ECM stiffness can be physiologically relevant, as matrices differently affected the commitment of stem cells grown on the top (Supplementary Fig. S2), a process that is directed by matrix elasticity (27). Therefore, our data indicate that TGFβ-activated fibroblasts require Snail1 expression to generate stiff ECMs with highly organized fibers.

Snail1 controls myofibroblastic signaling

Protein expression analysis provided further support that Snail1 is required for major changes of the 3D-ECM: In the absence of Snail1, the total amount of extracellular molecules, such as fibronectin, thrombospondin, and lysyl oxidase (LOX), was only weakly expressed and modulated by TGFβ (Fig. 2A). We also analyzed whether Snail1 was required for the expression of αSMA, the actin isoform that provides high contraction power to stress fibers involved in fibronectin fibrillogenesis and ECM remodeling. In control fibroblasts, Snail1 accumulated in response to TGFβ, with a peak at 1 hour, whereas the myofibroblast marker αSMA progressively accumulated at later times (e.g., at 8 and 24 hours; Fig. 2B). In contrast, in the absence of Snail1, αSMA levels were not efficiently induced by TGFβ (Fig. 2B). In agreement with the αSMA protein levels, TGFβ promoted the formation of αSMA-positive stress fibers in 85% of control MEFs, but only in 10% of KO MEFs (Fig. 2C). αSMA and fibronectin fibers frequently coaligned in control MEFs treated with TGFβ (Supplementary Fig. S3A). The length of the paxillin-stained focal contacts (Supplementary Fig. S3B and S3C) and the fibronectin fibrillogenesis capacity (Fig. 2D) of the fibroblasts were also Snail1 and TGFβ dependent. Because αSMA expression and stress fiber contraction are RhoA-dependent events, we analyzed RhoA activity. We detected that active RhoA–GTP was higher in control MEFs than in KO MEFs, and that the lack of Snail1 prevented full RhoA activation by TGFβ (Fig. 3A). These data suggest that Snail1 is required for TGFβ-induced RhoA/αSMA–dependent mechanisms that direct ECM organization. Indeed, similar to *Snai1* depletion, a specific inhibitor of the RhoA pathway, Y23762, prevented the TGFβ-induced accumulation of αSMA (Fig. 3B) and the orientation of fibronectin fibers and nuclei (Fig. 3C and D). Furthermore,

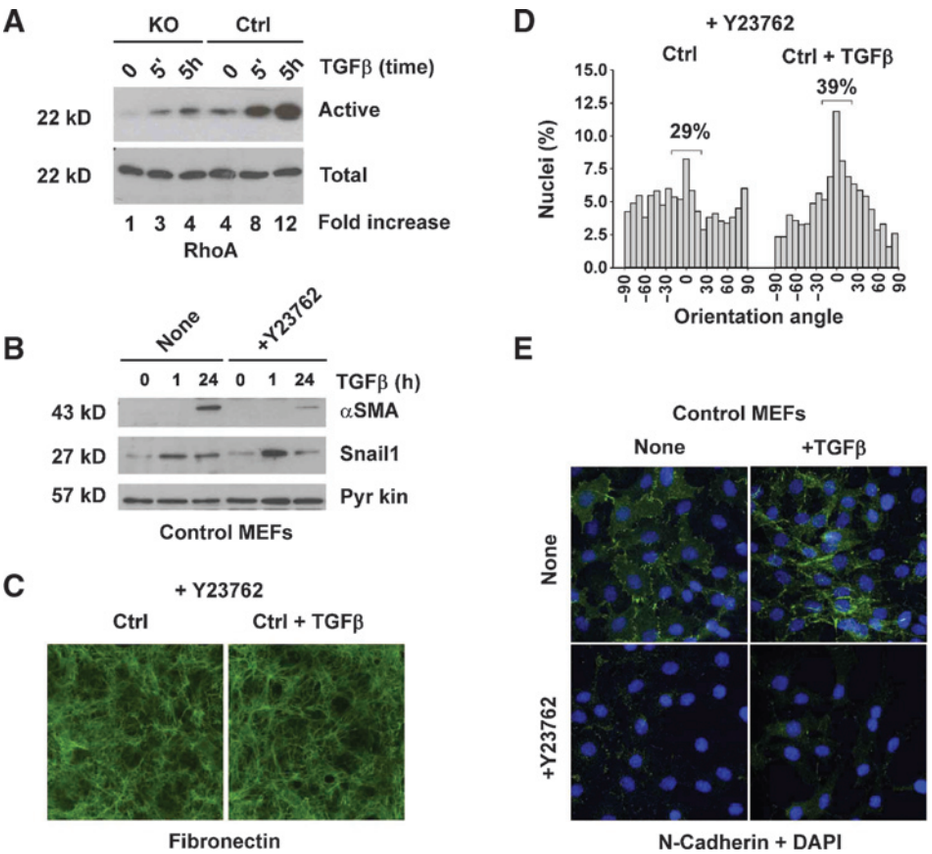

Figure 3.

Snail1 is required for RhoA activity. A, active RhoA-GTP in MEFs. Protein extracts from MEFs treated with TGFβ (5 ng/mL) for the times indicated were used in a GST–Rhotekin pull-down analyzed by Western blot analysis. Active RhoA (RhoA-GTP in pull-down) normalized by total RhoA (RhoA in input) was quantified by densitometry from a representative experiment, and the fold increase relative to the amount in nontreated KO MEFs is shown. B, time course of Snail1 and αSMA expression in the presence of a ROCK1 inhibitor (Y23762). The experiment was performed and analyzed as in Fig. 2A but using control MEFs grown in the presence or absence of 10 μmol/L of Y23762. C, fibronectin fibers in 3D-ECMs generated in the presence Y23762. The experiment was performed and analyzed as in Fig. 1A but using control MEFs grown in the presence or absence of 10 μmol/L of Y23762. D, nuclei orientation of MEFs grown in the presence of Y23762. Nuclei of MEFs used in C were analyzed as in Fig. 1C. E, N-cadherin localization in control MEFs in the presence of the ROCK1 inhibitor Y23762. N-Cadherin (green) and nuclei (blue) were visualized by immunofluorescence (×200) in the indicated MEFs grown for 24 hours on plastic dishes in the presence or absence of 10 μmol/L of Y23762.

Y23762 treatment prevented the formation of mature N-cadherin contacts (Fig. 3E), which are myofibroblast-associated cell-to-cell junctions that we also found to be TGFβ and Snail1 dependent (Supplementary Fig. S4). In contrast, the inhibitor did not prevent the rapid increase of Snail1 levels (Fig. 3B). Altogether, our data indicate that Snail1 is needed for the TGFβ molecular pathway that promotes the myofibroblastic RhoA/αSMA–dependent remodeling of the intracellular cytoskeleton and ECM.

Snail1 depletion prevents myofibroblast activation and ECM organization during wound healing

In the context of adult skin, only wound-healing fibroblasts at the granulation tissue were found to express Snail1 (19). Thus, to test whether physiologic myofibroblasts require Snail1 to remodel the ECM, controlled wounds were made in the skin of tamoxifen-pretreated control (*Snai1*$^{+/flox}$) and Snail1 KO (tamoxifen-inducible *Snai1*$^{-/flox}$ knockdown) mice. Healing for several days revealed that wound closure was clearly delayed in KO animals (Fig. 4A). In the 5-day wounds of control animals, Snail1 and αSMA were detected in spindle-shaped cells of the granulation tissue (Fig. 4B), which had parallel fibronectin fibers oriented toward the wound (Fig. 4C). Besides depleting *Snai1* in KO animals, tamoxifen severely decreased αSMA expression, collagen deposition (Fig. 4B), and fibronectin alignment (Fig. 4C). Fibroblast organization within the granulation tissue was estimated by calculating the orientation angle of DAPI-stained nuclei. In control animals, 80% of the cells aligned together with the parallel fibronectin fibers (Fig. 4C), whereas in *Snai1*-depleted mice, cells oriented randomly. Therefore, these data indicate that physiologic wound-healing myofibroblasts express Snail1, and that myofibroblast-dependent activities, such as structuration of granulation tissue and wound repair, are disturbed in the absence of Snail1.

Snail1 levels in human primary CAFs correlate with their capability to organize the ECM

The presence of tumor cells triggers a desmoplastic response in the stroma that is similar to that of wound healing but is mainly conducted by CAFs. Thus, we evaluated whether human primary CAFs from surgical colon tumors express Snail1 and generate organized 3D-ECMs. Three different established lines of CAFs (#77, #120, and #148) were analyzed by Western blot analysis. Snail1 expression was higher in CAF #120 than in the other two lines, and the expression of other proteins characteristic for activated fibroblasts, such as αSMA, fibronectin, and N-cadherin, nicely correlated with the levels of Snail1 (Fig. 5A). Fibronectin fibers in 3D-ECMs and the nuclei of the three CAFs lines showed anisotropic orientation, although to different extents: Whereas CAF #120 presented a highly orientated distribution, the other two lines showed a lower degree of orientation (Fig. 5B). The anisotropy of 3D-ECM fibers generated by CAF #120 with high levels of Snail1 mimicked that generated by TGF-β–activated

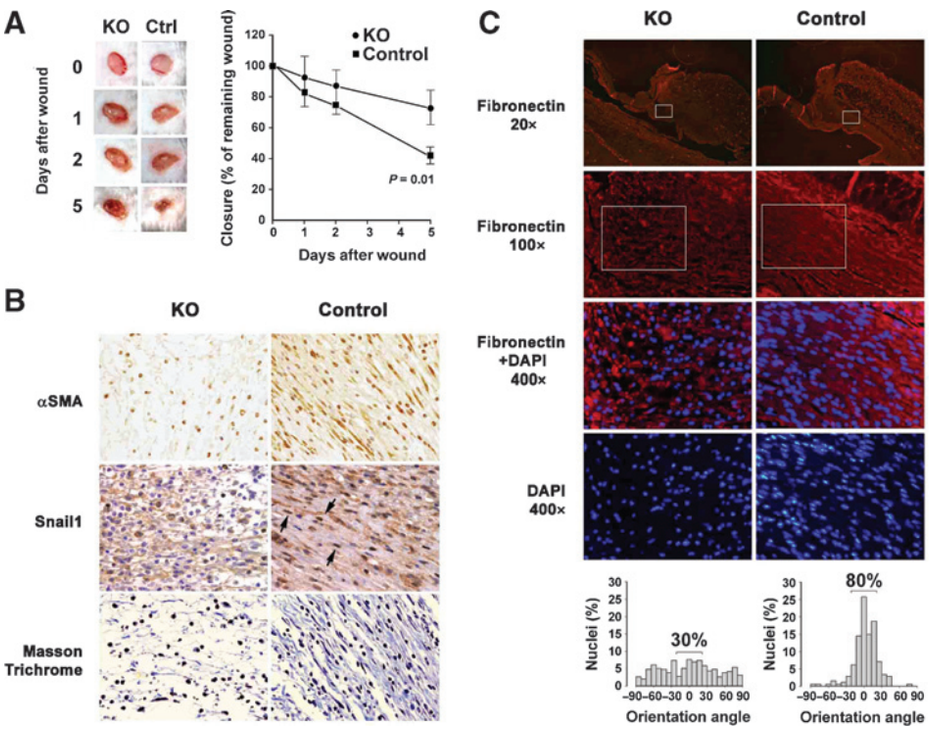

Figure 4.
Snail1-deficient mice display ECM defects related to myofibroblast activity in wound healing. A, skin wound healing in control and *Snai1*-deficient mice. *Snai1*$^{+/flox}$ (control) and *Snai1*$^{+/flox}$ (KO) mice were treated with tamoxifen, and skin wounds (6 mm in diameter) were made after 10 days. Photographs of representative wounds on the indicated days are shown. Plot represents the mean ± SD for the percentage of closure from a minimum of six wounds performed on different animals. The Student *t* test *P* value is indicated. B, αSMA, Snail1, and Masson's trichrome in the hypodermis adjacent to skin wounds. Five-day wounds from tamoxifen-treated control and KO mice were analyzed by immunohistochemistry and visualized at ×400. Arrows, spindle-shaped cells positive for nuclear Snail1.
C, fibronectin and nuclei staining in the hypodermis adjacent to skin wounds. Five days wounds were analyzed by immunofluorescence. Fibronectin (red) and DAPI stained (blue) were visualized at the indicated magnifications. The orientation angles of DAPI-visualized nuclei were analyzed as in Fig. 1C.

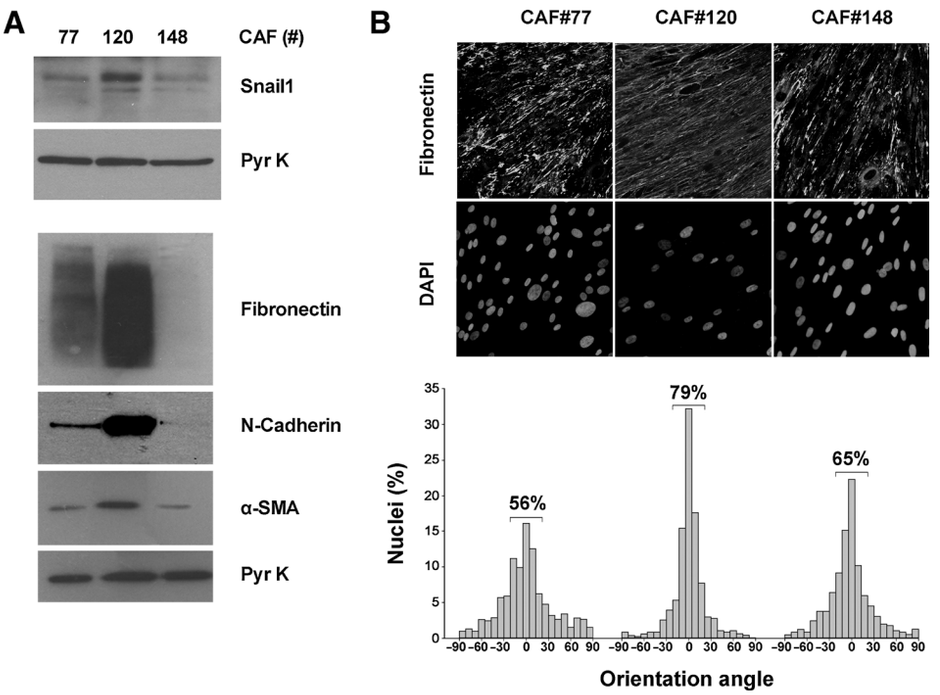

Figure 5.
Snail1 levels determine the capacity of CAF lines established from surgical human tumors to reorganize the ECM matrix. A, protein expression in primary CAF lines. Fibronectin, αSMA, Snail1, N-cadherin, and pyruvate kinase from indicated CAF lines were measured from total cell extracts by Western blot analysis. B, fibronectin fibers in 3D-ECMs and nuclei orientation of primary CAFs. CAF lines were grown according to the standard protocol for generating 3D-ECMs. Fibronectin and CAF nuclei were visualized and nuclei orientation was analyzed as in Fig. 1C (bottom).

control but not by KO MEFs, and it recapitulates the ECM observed in granulation tissue of control but not Snail1 KO mice. Therefore, these data from CAFs are consistent with Snail being required for ECM modeling and show that the Snail1 levels are indicative of the CAF activity on ECM orchestration.

ECM produced by s*nai1*-defective fibroblasts fails to promote anisotropic cancer cell migration and invasion

To analyze whether matrices influence tumor cell behavior in a Snail1-dependent manner, we studied the migratory capacity of tumor cells on 3D-ECMs generated in the absence of Snail1. Tumor cells plated on decellularized 3D-ECM generated by control MEFs acquired an amoeboid morphology (Fig. 6A) with a "lymphocytic" type of movement, as nuclei of these cells oriented randomly (Fig. 6A) and moved without a preferential direction (Fig. 6B; Supplementary Video S1). However, when plated on top of a 3D-ECM from control MEFs treated with TGFβ (following the protocol used in Fig. 1), the tumor cells acquired a bipolar fusiform morphology, and their nuclei orientation and movement were anisotropic (Fig. 6A and B; Supplementary Video S2), even though no TGFβ was added. These effects on tumor cells were not sustained by ECM from Snail1-depleted fibroblasts (Fig. 6A and B; Supplementary Videos S3 and S4). Equivalent results were observed for tumor cells from breast and pancreas origin (Supplementary Videos S1–S8).

We further analyzed whether activated fibroblast-derived 3D-ECMs were more suitable for tumor cell invasion. Decellularized 10-day-old 3D-ECMs were generated on Boyden Chambers inserts, and tumor cells were seeded on top of them to assay their invasive capacity. Indeed, matrices derived from control cells were more susceptible for invasion than those derived from KO cells, especially after TGF-β treatment (Fig. 6C). Therefore, these data indicate that the presence of Snail1 in activated fibroblasts is required to generate an ECM that promotes tumor anisotropic migration and facilitates invasion.

Snail1 expression in breast cancer stroma induces local anisotropic fibronectin and collagen alignment and is associated with a poor outcome

To directly estimate the relevance of Snail1 expression on the architecture of the tumor stroma and cancer malignance, we analyzed by immunohistochemistry the Snail1 expression in the stroma of 371 human early breast-infiltrating carcinomas. We found that 61 cases (16.4%) had Snail1 nuclear expression in stromal spindle-shaped cells (Supplementary Table S1). Subsequently, we analyzed the fibronectin and collagen alignment in the connective tissue in a set of tumors (15 with Snail1-positive stroma, and 15 with a Snail1-negative stroma). Both fibronectin fibers visualized by immunohistochemistry (Fig. 7A, top) and collagen fibers visualized by second harmonic generation (SHG; Fig. 7B), aligned perpendicularly to tumors in stromal areas with Snail1-positive cells. In contrast, no oriented fibers were observed in areas without Snail1-positive fibroblasts or in tumor samples negative for Snail1 in stroma (Fig. 7A, bottom).

Anisotropic fibronectin fiber alignment (Fig. 7A, middle) and fibroblast orientation in the stroma (Fig. 7C) were observed despite the presence of variable amounts of Snail1-negative fibroblasts intermingled with positive ones. For this reason, we tested whether Snail1-expressing CAFs organize the ECM in the presence of nonactivated MEFs. Mixed cultures with 30% of CAF #120 promoted fibronectin alignment to a similar degree observed in 3D-ECMs generated by CAF #120 alone, whereas lower percentages promoted a local realignment (Fig. 7D). The same dominant effect of CAF#120 was observed when MEF orientation was measured in cocultures by taking advantage of the fact that DAPI-stained murine nuclei are distinguishable from human CAF nuclei (Fig. 7D and Supplementary Fig. S5A). Furthermore, by analyzing nuclei alignment of MEFs grown in the presence of 30% of the different CAF lines, we found that MEF orientation correlated with the levels of Snail1 expressed by the CAF lines (Fig. 7E and Supplementary Fig. S5B).

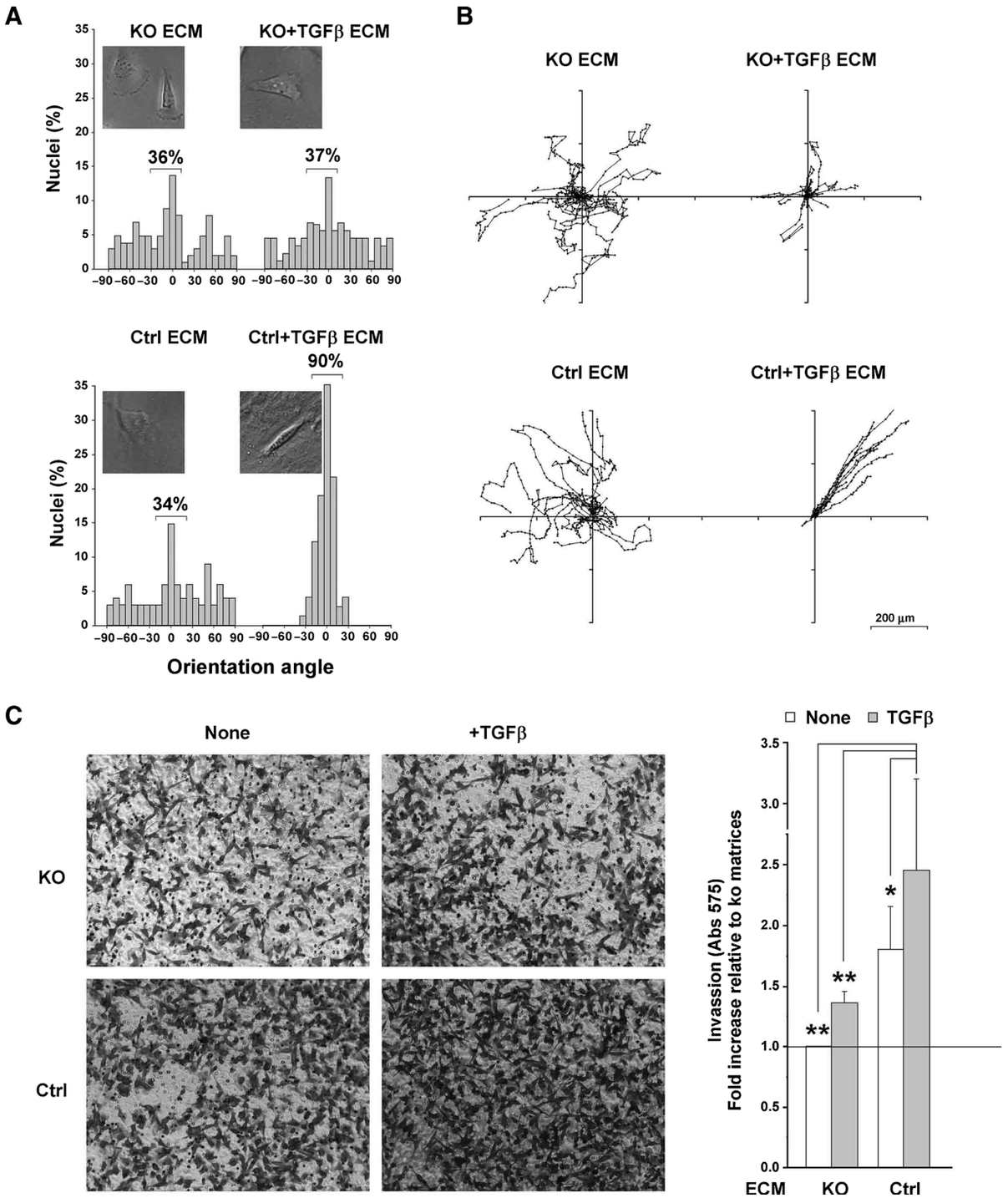

Figure 6.
ECM matrices generated in the absence of Snail1 prevent directional migration and effective invasion. A, nuclei orientation of MDA-MB-231 tumor cells grown on 3D-ECMs. Cells plated on the indicated decellularized matrices were allowed to attach for 24 hours. Nuclei of tumor cells were stained with DAPI, and nuclei orientation angles were calculated and plotted as in Fig. 1. A transmitted light image of a representative cell grown in the indicated 3D-ECM is shown. B, single-cell tracks of MDA-MB-231 tumor cells moving on 3D-ECM. Cell tracker–labeled green cells plated on decellularized matrices generated by the indicated MEFs were allowed to attach for 24 hours and then photographed every 15 minutes over a period of 16 hours. Single-cell coordinates at each time point were calculated with ImageJ, and tracks of ten representative cells per condition relative to the initial position were plotted. C, invasive capacity of MDA-MB-231 cells on 3D-ECM. Cell tracker–labeled green cells were plated on decellularized matrices generated on invasion inserts by the indicated MEFs and allowed to invade the matrices for another 24 hours. Images (×100) of crystal violet–stained cells attached to the lower side of the membrane are shown. Cells were then quantified by measuring the A575 of the cells solubilized with an HCl solution. Values represent the mean ± SD from three independent experiments. Asterisks indicate a statistically significant difference as determined by the Student *t* test with *, $P < 0.05$ and **, 0.01.

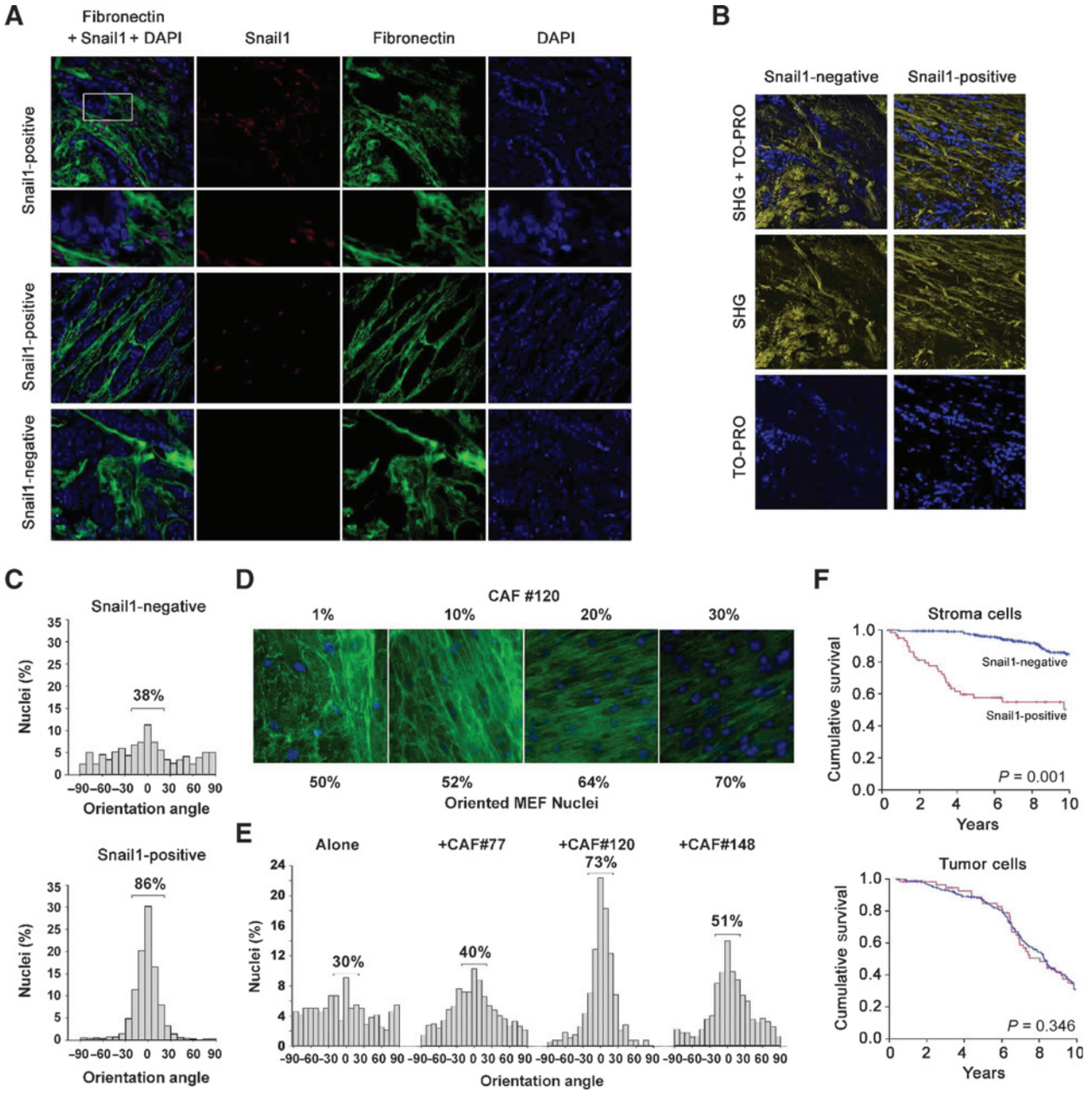

Figure 7.

The presence of Snail1-expressing fibroblasts in desmoplasic areas of breast cancers correlates with a decreased OS and with local anisotropic fibronectin and collagen alignment. A and B, fiber organization in stromal areas of representative tumors with positive (top and middle) and negative (bottom) Snail1 staining. A, fibronectin (green) and Snail1 (red) were visualized (×400) by multispectral immunofluorescence. Nuclei (blue) were stained with DAPI. For the top, an electronic amplification (×3) of the indicated box is shown. B, samples from the same tumors as in A were used to visualize collagen fibers by SGH (yellow). Nuclei (blue) were stained with TO-PRO. C, nuclei orientation of fibroblast from tumor specimens with Snail1-positive or -negative stroma. The nuclei orientation angles of fibroblasts from eight tumors per condition (more than 500 fibroblasts) were calculated and plotted as in Fig. 1C. D, MEF nuclei reorientation in the presence of increasing amounts of CAF #120. Control MEFs were grown according to the standard protocol for generating 3D-ECMs in the presence of increasing amounts of CAF #120. The final percentage of CAFs relative to the total amount of fibroblasts in the coculture was estimated by counting a minimum of 500 nuclei per condition. MEF nuclei angles in the cocultures were calculated as indicated in Supplementary Fig. S5A and the percentage of oriented nuclei is indicated at the bottom. E, nuclei orientation of MEFs grown in the presence of primary CAF lines. Nuclei were stained with DAPI from cocultures of control MEFs and the indicated CAF lines. The nuclei orientation angles of MEFs were calculated (for more details, see Supplementary Fig. S5A–S5B) and plotted as in Fig. 1C. F, Kaplan–Meier cumulative curves for OS in patients with early breast cancer according to Snail1 expression in the stroma (top plot) and in the tumor (bottom plot). The *P* values are indicated.

The presence of Snail1-positive fibroblasts in the stromal compartment directly correlated with lymph node involvement at diagnosis ($P = 0.033$; Supplementary Table S1) and associated with poor overall survival [OS; HR, 5.31; 95% confidence interval (CI), 3.14–8.99; $P = 0.001$; Fig. 7F; Supplementary Table S2]. In contrast, no significant differences in OS were observed for the

expression of Snail1 in tumor cells ($P = 0.364$; Fig. 7F). Moreover, the significance of Snail1 expression in stroma was maintained in a Cox multivariate analysis for OS (HR, 4.54; 95% CI, 2.53–8.15; $P = 0.001$; Supplementary Table S2). Therefore, our data demonstrate that the presence of scattered Snail1-expressing fibroblasts in the stroma of human early breast cancers is a *bona fide* marker of lymph node involvement and poor cancer outcome associated to a myofibroblastic ECM that acts as a mechanical prometastatic stroma.

Discussion

Although Snail1 is known to trigger EMT (18), a plasticity process providing tumor epithelial cells with invasive capacity, Snail1 expression and its consequences in carcinomas are controversial, with a few studies for breast cancer (28–30) and other cancers (31, 32) reporting no significant association to patient survival. Here, we found that Snail1 expression in the tumor stroma, rather than in epithelial cells, associates with lymph node metastasis at diagnosis and has a robust prognostic value for early breast-infiltrating carcinomas. This result is in agreement with a previous study, indicating that fibroblastic Snail1 expression predicts outcome of colon cancer (20). Indicative of the role of fibroblastic Snail1 in breast cancer, we found that tumor stroma containing Snail1-expressing fibroblasts presented a characteristic alignment of the fibronectin fibers and a collagen alignment signature that was reported to predict breast cancer patient outcome (13). Indeed, our data from cultured fibroblast show that Snail1 is required for the generation of ECMs with anisotropic fibers and elevated rigidity, two biophysical parameters that independently affect cell migration (33) and support cancer invasion and malignance (10, 11). Thus, fibroblastic Snail1 can influence not only the cytokine profile secreted by CAFs, as recently described for colon tumor cells (22), but also the extracellular mechanical cues that facilitate and guide tumor invasion.

Using control and Snail1-deficient MEFs activated with TGFβ, we demonstrated that Snail1 stimulates the myofibroblastic RhoA/αSMA axis that sustains maturation of cell–cell and cell–surface contacts, fibronectin fibrillogenesis, and eventually ECM alignment. Primary CAF lines also produced such ordered matrices in the absence of exogenous TGFβ, in line with the observation that CAFs are endowed with a TGFβ feedback loop (14, 34). However, this is only a general observation, because CAFs were shown to be a heterogeneous population of fibroblasts when studied in detail (35). Accordingly, the three CAF lines used in this study presented variable ECM organization that correlated with the levels of Snail1 and αSMA they express. Therefore, the amount of Snail1 expressed by a particular CAF is indicative of its capacity to remodel the ECM. Remarkably, we show that this capacity is dominant. In organized stromal areas of human tumors, Snail1-expressing CAFs were observed to be scattered among Snail1-negative ones and, in cocultures, nonactivated fibroblasts were "educated" to rearrange the matrix by few Snail1-positive CAFs. These observations describing the capacity of an heterogeneous population of fibroblasts to produce an homogeneous architectural outcome fit with results proving that matrices generated by CAFs contain topographic and molecular information for triggering desmoplastic differentiation of normal fibroblasts (36).

A consequence of the cytoskeletal activity imposed by the TGFβ/Snail1/RhoA mechanism is that molecules such as fibronectin, αSMA, and N-cadherin are incorporated and accumulated into stable fibers or cell contacts. Therefore, Snail1 modulates the levels of these structural molecules in myofibroblasts at distinct levels: transcriptionally, acting as a coactivator of TGFβ-induced ECM genes (23), and posttranscriptionally, inducing protein stabilization through this RhoA-dependent mechanism. The protein levels of LOX, the collagen crosslinking enzyme essential to generate stiffer ECMs (37), also increased in a Snail1-dependent manner. It is likely that the Snail1 effect on both ECM fiber accumulation and LOX activity are behind the increased ECM rigidity. Rigidity increments from 0.8 to 4 kPa (in the range modulated by Snail1 and TGFβ in our AFM measurements) have been described for the connective tissue of breast tumors (38), and are associated to a bad prognosis (10). Therefore, Snail1-expressing CAFs have the potential to increase ECM stiffness, which promotes breast cancer invasion.

On the basis of the discussed data and the observation that interfering with LOX activity by shRNAs or inhibitors (unpublished data) did not prevent fibronectin alignment in 3D-ECMs, we envision the process of breast cancer stroma remodeling to be initiated by Snail1/RhoA–dependent fibronectin fibrillogenesis. The resulting aligned fibronectin fibers work as a template for the assembly of other extracellular molecules, including collagen. Collagen fibers are subsequently cross-linked by LOX, fixing and hardening the ECM fiber network. Given that collagen-activated DDR receptors prevent Snail1 degradation (39), a positive feedback loop maintaining stable Snail1 and ECM fiber topology and rigidity is likely to be sustaining activated stroma. Our data suggest a model that places fibroblastic Snail1 in the core of the mechanical signaling regulation and explains better than any other why a TGFβ-driven program in stromal cells predicts tumor outcome (15). The molecular determinants involved in the activation of RhoA by TGFβ have not yet been deciphered. It is likely that one or several repressors of the RhoA activity (RhoA-GAPs or –GDIs) are simultaneously inhibited by rapid TGFβ receptor–dependent phosphorylation and Snail1-dependent transcriptional repression. In this way, either the absence of Snail1 or the lack of TGFβ treatment would be sufficient to prevent full RhoA activation, as our data show.

Cancers have been considered to be "wounds that never heal," in reference to the fact that the desmoplastic response that is transient in wounds is sustained in tumors. Our data show that Snail1-deficient mice had fibronectin fibers in the granulation tissue of skin wounds that did not adopt a proper parallel alignment, and that their wound closure was slower. Indeed, a similar delay was observed in mice with a low expression of endogenous TGFβ or with the TGFβ receptor in the granulation tissue (40), suggesting that both TGFβ and Snail1 are required for the myofibroblastic activity in reorganizing granulation tissue. We propose that Snail1 mediates an ECM-related TGFβ-signaling branch that allows myofibroblasts in either the granulation tissue or the tumor stroma to assemble a rigid and fiber-aligned ECM. This architecture promotes and guides the epithelial cell movements required for both wound closure and tumor invasion. Moreover, because fibrosis emulates an uncontrolled wound repair, it is likely that exacerbated TGFβ/Snail1/RhoA signaling supports it. Indeed, ECM deposition in hepatic fibrosis is Snail1 dependent (41), and Snail1 is required for hepatocyte and lung fibrosis progression (41, 42). Therefore, interfering with this Snail1-dependent pathway could provide a way to palliate the effects of these devastating disorders and cancers.

Disclosure of Potential Conflicts of Interest

No potential conflicts of interest were disclosed.

Authors' Contributions

Conception and design: J. Stanisavljevic, F. Bonilla, A. García de Herreros, J. Baulida

Development of methodology: J. Stanisavljevic, M. Herrera, C. Peña, D. Navajas, F. Rojo

Acquisition of data (provided animals, acquired and managed patients, provided facilities, etc.): J. Stanisavljevic, J. Loubat-Casanovas, T. Luque, A. Lluch, J. Albanell, A. Rovira, C. Peña, D. Navajas, F. Rojo

Analysis and interpretation of data (e.g., statistical analysis, biostatistics, computational analysis): J. Stanisavljevic, T. Luque, R. Peña, D. Navajas, F. Rojo, A. García de Herreros

Writing, review, and/or revision of the manuscript: J. Stanisavljevic, A. Lluch, J. Albanell, F. Bonilla, D. Navajas, F. Rojo, A. García de Herreros, J. Baulida

Administrative, technical, or material support (i.e., reporting or organizing data, constructing databases): J. Stanisavljevic, M. Herrera, R. Peña, A. Rovira

Study supervision: J. Albanell, J. Baulida

Acknowledgments

The authors thank Drs. Saurav Basu and Gustavo K. Rohde (Carnegie Mellon University, Pittsburgh, PA) for fibronectin alignment analysis, Dr. Xavier Sanjuan (Centre de Recerca Genòmica, Barcelona, Spain) for setting up SHG analysis, and Dr. Raquel Batlle (Institut de Recerca Biomèdica, Barcelona, Spain) for assistance in obtaining MSCs.

Grant Support

This work was supported by the Fondo de Investigaciones Sanitarias of the Instituto Carlos III (ISCIII; PI12/00257 to J. Baulida; PI12/00680 to J. Albanell; PI12/01552 to F. Rojo; and PI12/01421 to A. Lluch), the Fundación Científica de la Asociación Española contra el Cáncer (A.G. de Herreros), Ministerio de Ciencia y Tecnología (SAF2010-16089; A.G. de Herreros), Fundació La Marató de TV3 (A.G. de Herreros and F. Bonilla), the Spanish Ministry of Economy and Competitiveness FIS-PI11/00089 (D. Navajas), and the European Commission COST Action TD-1002 (D. Navajas). This work was also supported by ISCIII/FEDER (RD12/0036/0005, RD12/0036/0041, RD12/0036/0051, RD12/0036/0070, and PT13/0010/0012) and the Generalitat de Catalunya (2014SGR740 and 2014SGR32).

The costs of publication of this article were defrayed in part by the payment of page charges. This article must therefore be hereby marked advertisement in accordance with 18 U.S.C. Section 1734 solely to indicate this fact.

Received July 2, 2014; revised September 26, 2014; accepted October 15, 2014; published OnlineFirst December 8, 2014.

References

1. Hinz B. The myofibroblast: paradigm for a mechanically active cell. J Biomech 2010;43:146–55.
2. Lorena D, Uchio K, Alto Costa AM, Desmouliere A. Normal scarring: importance of myofibroblasts. Wound Repair Regen 2002;10:86–92.
3. Singh P, Carraher C, Schwarzbauer JE. Assembly of fibronectin extracellular matrix. Annu Rev Cell Dev Biol 2010;26:397–419.
4. Kii I, Nishiyama T, Li M, Matsumoto K-I, Saito M, Amizuka N, et al. Incorporation of tenascin-C into the extracellular matrix by periostin underlies an extracellular meshwork architecture. J Biol Chem 2010;285:2028–39.
5. Kadler KE, Hill A, Canty-Laird EG. Collagen fibrillogenesis: fibronectin, integrins, and minor collagens as organizers and nucleators. Curr Opin Cell Biol 2008;20:495–501.
6. Hinz B, Pittet P. Myofibroblast development is characterized by specific cell–cell adherens junctions. Mol Biol 2004;15:4310–20.
7. Khatau SB, Hale CM, Stewart-Hutchinson PJ, Patel MS, Stewart CL, Searson PC, et al. A perinuclear actin cap regulates nuclear shape. Proc Natl Acad Sci U S A 2009;106:19017–22.
8. Tripathi M, Billet S, Bhowmick NA. Understanding the role of stromal fibroblasts in cancer progression. Cell Adh Migr 2012;6:231–5.
9. Halder G, Dupont S, Piccolo S. Transduction of mechanical and cytoskeletal cues by YAP and TAZ. Nat Rev Mol Cell Biol 2012;13:591–600.
10. Levental KR, Yu H, Kass L, Lakins JN, Egeblad M, Erler JT, et al. Matrix crosslinking forces tumor progression by enhancing integrin signaling. Cell 2009;139:891–906.
11. Goetz JG, Minguet S, Navarro-Lérida I, Lazcano JJ, Samaniego R, Calvo E, et al. Biomechanical remodeling of the microenvironment by stromal caveolin-1 favors tumor invasion and metastasis. Cell 2011;146:148–63.
12. Provenzano PP, Inman DR, Eliceiri KW, Knittel JG, Yan L, Rueden CT, et al. Collagen density promotes mammary tumor initiation and progression. BMC Med 2008;6:11.
13. Conklin MW, Eickhoff JC, Riching KM, Pehlke CA, Eliceiri KW, Provenzano PP, et al. Aligned collagen is a prognostic signature for survival in human breast carcinoma. Am J Pathol 2011;178:1221–32.
14. Kojima Y, Acar A, Eaton EN, Mellody KT, Scheel C, Ben-Porath I, et al. Autocrine TGF-beta and stromal cell-derived factor-1 (SDF-1) signaling drives the evolution of tumor-promoting mammary stromal myofibroblasts. Proc Natl Acad Sci U S A 2010;107:20009–14.
15. Calon A, Espinet E, Palomo-Ponce S, Tauriello DVF, Iglesias M, Céspedes MV, et al. Dependency of colorectal cancer on a TGF-β-driven program in stromal cells for metastasis initiation. Cancer Cell 2012;22:571–84.
16. Raftopoulou M, Hall A. Cell migration: Rho GTPases lead the way. Dev Biol 2004;265:23–32.
17. Kardassis D, Murphy C, Fotsis T, Moustakas A, Stournaras C. Control of transforming growth factor beta signal transduction by small GTPases. FEBS J 2009;276:2947–65.
18. García de Herreros A, Baulida J. Cooperation, amplification, and feed-back in epithelial–mesenchymal transition. Biochim Biophys Acta 2012;1825:223–8.
19. Francí C, Takkunen M, Dave N, Alameda F, Gómez S, Rodríguez R, et al. Expression of Snail protein in tumor-stroma interface. Oncogene 2006;25:5134–44.
20. Francí C, Gallén M, Alameda F, Baró T, Iglesias M, Virtanen I, et al. Snail1 protein in the stroma as a new putative prognosis marker for colon tumours. PLoS ONE 2009;4:e5595.
21. Rowe RG, Li X-Y, Hu Y, Saunders TL, Virtanen I, Garcia de Herreros A, et al. Mesenchymal cells reactivate Snail1 expression to drive three-dimensional invasion programs. J Cell Biol 2009;184:399–408.
22. Herrera A, Herrera M, Alba-Castellón L, Silva J, García V, Loubat-Casanovas J, et al. Protumorigenic effects of Snail-expression fibroblasts on colon cancer cells. Int J Cancer 2014;134:2984–90.
23. Stanisavljevic J, Porta-de-la-Riva M, Batlle R, de Herreros AG, Baulida J. The p65 subunit of NF-κB and PARP1 assist Snail1 in activating fibronectin transcription. J Cell Sci 2011;124:4161–71.
24. Batlle R, Alba-Castellón L, Loubat-Casanovas J, Armenteros E, Francí C, Stanisavljevic J, et al. Snail1 controls TGF-β responsiveness and differentiation of mesenchymal stem cells. Oncogene 2013;32:3381–9.
25. Domínguez D, Montserrat-Sentís B, Virgós-Soler A, Guaita S, Grueso J, Porta M, et al. Phosphorylation regulates the subcellular location and activity of the snail transcriptional repressor. Mol Cell Biol 2003;23:5078–89.
26. Herrera M, Islam ABMMK, Herrera A, Martín P, García V, Silva J, et al. Functional heterogeneity of cancer-associated fibroblasts from human colon tumors shows specific prognostic gene expression signature. Clin Cancer Res 2013;19:5914–26.
27. Engler AJ, Sen S, Sweeney HL, Discher DE. Matrix elasticity directs stem cell lineage specification. Cell 2006;126:677–89.
28. Lundgren K, Nordenskjöld B, Landberg G. Hypoxia, Snail and incomplete epithelial–mesenchymal transition in breast cancer. Br J Cancer 2009;101:1769–81.
29. Nassar A, Sookhan N, Santisteban M, Bryant SC, Boughey JC, Giorgadze T, et al. Diagnostic utility of snail in metaplastic breast carcinoma. Diagn Pathol 2010;5:76.
30. Montserrat N, Gallardo A, Escuin D, Catasus L, Prat J, Gutiérrez-Avignó FJ, et al. Repression of E-cadherin by SNAIL, ZEB1, and TWIST in invasive

ductal carcinomas of the breast: a cooperative effort? Hum Pathol 2011;42:103–10.
31. Häyry V, Mäkinen LK, Atula T, Sariola H, Mäkitie A, Leivo I, et al. Bmi-1 xpression predicts prognosis in squamous cell carcinoma of the tongue. Br J Cancer 2010;102:892–7.
32. Kroepil F, Fluegen G, Vallböhmer D, Baldus SE, Dizdar L, Raffel AM, et al. Snail1 expression in colorectal cancer and its correlation with clinical and pathological parameters. BMC Cancer 2013;13:145.
33. Pathak A, Kumar S. Independent regulation of tumor cell migration by matrix stiffness and confinement. Proc Natl Acad Sci U S A 2012;109:10334–9.
34. Hawinkels LJAC, Paauwe M, Verspaget HW, Wiercinska E, van der Zon JM, van der Ploeg K, et al. Interaction with colon cancer cells hyperactivates TGF-β signaling in cancer-associated fibroblasts. Oncogene 2014;33:97–107.
35. Sugimoto H, Mundel TM, Kieran MW, Kalluri R. Identification of fibroblast heterogeneity in the tumor microenvironment. Cancer Biol Ther 2006; 5:1640–6.
36. Amatangelo MD, Bassi DE, Klein-Szanto AJP, Cukierman E. Stroma-derived three-dimensional matrices are necessary and sufficient to promote desmoplastic differentiation of normal fibroblasts. Am J Pathol 2005;167: 475–88.
37. Taylor MA, Amin JD, Kirschmann DA, Schiemann WP. Lysyl oxidase contributes to mechanotransduction-mediated regulation of transforming growth factor-β signaling in breast cancer cells. Neoplasia 2011;13: 406–18.
38. Butcher DT, Alliston T, Weaver VM. A tense situation: forcing tumour progression. Nat Rev Cancer 2009;9:108–22.
39. Zhang K, Corsa CA, Ponik SM, Prior JL, Piwnica-Worms D, Eliceiri KW, et al. The collagen receptor discoidin domain receptor 2 stabilizes SNAIL1 to facilitate breast cancer metastasis. Nat Cell Biol 2013;15:677–87.
40. Peters T, Sindrilaru A, Hinz B, Hinrichs R, Menke A, Al-Azzeh EAD, et al. Wound-healing defect of CD18(−/−) mice due to a decrease in TGF-beta1 and myofibroblast differentiation. EMBO J 2005;24:3400–10.
41. Rowe RG, Lin Y, Shimizu-Hirota R, Hanada S, Neilson EG, Greenson JK, et al. Hepatocyte-derived Snail1 propagates liver fibrosis progression. Mol Cell Biol 2011;31:2392–403.
42. Balli D, Ustiyan V, Zhang Y, Wang I-C, Masino AJ, Ren X, et al. Foxm1 transcription factor is required for lung fibrosis and epithelial-to-mesenchymal transition. EMBO J 2013;32:231–44.
43. Basu S, Liu C, Rohde GK. Localizing and extracting filament distributions from microscopy images. Journal of Microscopy, in press 2014.